

Spin Correlations in Top Production and Decay at e^+e^- Colliders

Andrew E. Blechman

Advisor: Professor Lynne H. Orr

Submitted as a senior thesis to the University of Rochester
in partial fulfillment of the requirements for the degree of
Bachelor of Science in Physics.

May, 2001

Abstract

The top quark, recently discovered at Fermilab, decays before it can hadronize; this allows its spin information to be passed directly to its daughter particles. We study these spin correlations in on-shell top production and decay at electron-positron colliders, looking at both dilepton and lepton+jets events. Using Monte Carlo techniques and the Spinor Helicity Method, we calculate tree-level cross sections in terms of quantities that are directly observable experimentally. We implement a reconstruction of the top quark momentum and consider how our reconstructed momentum changes the previously calculated results.

Acknowledgements

There are many people that I would like to thank that made this entire project possible. First and foremost, I thank Professor Lynne Orr, who offered me the wonderful opportunity to do a theoretical high-energy physics project as an undergraduate. I also want to thank the entire Phenomenology group for all of their help, especially Cosmin Macesanu, who wrote the original Monte Carlo used in this thesis and has been following along as I worked on my analysis, and on more than one occasion helped me to keep my head above water! Also Doreen Wackerth, who was invaluable in helping me make all my plots look nice in LaTeX.

On the broader side, I want to thank all of my professors that have taught me what it means to do physics. I especially want to thank Professor Thomas Ferbel, who on one fateful Sunday afternoon during my Sophomore year, convinced me to be a particle physicist. I am also indebted to all of my friends and fellow physics majors for all of their support over the last four years. A special thank you to Brock Tweedie for all of our great conversations about particle physics, and my housemate and old friend Daniel Rice, who on several occasions listened with good humor as I told him all of the things that were going wrong!

Finally, I would like to thank my family for all of their support: my parents, my sister Ilene and brother-in-law Kevin Krom, who has helped me several times with his computing knowledge.

The road goes ever on and on
Down from the door where it began.
Now far ahead the Road has gone,
And I must follow, if I can,
Pursuing it with weary feet,
Until it joins some other way,
Where many paths and errands meet.
And whither then? I cannot say.

–J. R. R. Tolkien, *Fellowship of the Ring*

1 Introduction

1.1 The Standard Model

The Standard Model of Particle Physics (SM) has had great success. Thus far, all of its predictions have been verified, but there are many reasons why particle physicists think that there is more to the story. One of the predictions that has only recently been confirmed is the existence of the “top” quark, the heaviest of all the fundamental constituents of matter. The top quark was discovered at the Tevatron Accelerator at the Fermi National Accelerator Laboratory (Fermilab). Two experiments, the Collider Detector Facility (CDF) and the $D\bar{0}$ Collaboration, independently reported finding the top quark with a mass of 176.8 ± 6.5 GeV/ c^2 and 173.3 ± 8.4 GeV/ c^2 respectively (see [1]). Many interesting questions still remain to be answered about the top quark. In this paper, we will be using the top system to consider spin correlations in the production and decay mechanisms.

The SM divides particles into two general categories: the force carriers and the matter particles. The force carriers are spin-1 bosons. They are responsible for mediating the forces between other particles. The photon (γ) is responsible for mediating the electromagnetic interaction, or Quantum Electrodynamics (QED). It couples to any particle that has electric charge. The massive vector bosons (W^\pm , Z^0) are responsible for mediating the weak interaction. The theory of Glashow, Weinberg and Salam (GWS) shows that the electromagnetic and weak interactions are actually different manifestations of the same force, called the “electroweak interaction”. This is important to keep in mind, since the electroweak interaction is responsible for top production in this study. Finally, the gluon (g) is responsible for mediating the strong interaction, or Quantum Chromodynamics (QCD); we not be directly concerned with QCD in this study.

The other types of particles in the SM are those that compose matter. The matter

particles are spin- $\frac{1}{2}$ fermions; they are subdivided into several types, based on their various properties and what forces they feel. One type of particle is the **lepton**, which is a particle that does not interact through QCD; i.e.: leptons do not couple to gluons. The leptons that we know of are the electron (e), the muon (μ), the tau (τ) and their corresponding neutrinos (ν_l). A generic lepton other than a neutrino will be denoted by “ l ”. With the exception of the neutrinos, leptons are negatively charged, and their antiparticles are positively charged, so they couple to photons as well as the massive vector bosons. Neutrinos, however, are neutral; therefore they *only* interact through the weak interaction. This makes them very difficult to see directly. However, their presence can be inferred by missing energy and momentum in the detector.

The other particles that compose matter in the SM are called **quarks**. These particles are different from leptons in that in addition to feeling the electroweak interaction, they also couple to gluons. This gives them many special properties. We know of six quarks (and their antiquark partners): those with electric charge $-\frac{1}{3}e$ are the down (d), strange (s) and bottom (b) quarks; those with electric charge $+\frac{2}{3}e$ are the up (u), charm (c) and top (t) quarks. A generic quark will be denoted by “ q ”, and antiquarks have bars over them (“ \bar{q} ”).

Because quarks feel the strong force, they cannot exist by themselves. This is because QCD is such a strong interaction that it is energetically favorable for a “naked quark” to pull another quark from the vacuum and create a color-neutral particle called a **hadron**. This process is called **hadronization**, and is a result of the QCD property of **quark confinement**. Therefore, when a quark is produced in a detector, it hadronizes almost immediately, and the result is a collimated shower of particles. This stream of particles from hadronization in a detector is called a **jet**. Common examples of hadrons are the protons and neutrons that make up a nucleus, and pions and K-mesons that are produced in cosmic rays and small accelerators.

However, this does *not* happen to the top quark. The reason is as follows: the time it takes for hadronization to occur is dictated by the QCD scale (Λ_{QCD}). However, because the top quark is so massive, its lifetime is shorter than the time scale set by Λ_{QCD} . Therefore, the top quark decays before it has time to hadronize, and so it decays as a naked quark. This is the only quark we know of that does not hadronize.

Because the top quark does not hadronize, its decay products carry all of the information the top quark carried. Normally, this is not the case: the hadronization process has the effect of smearing information. One characteristic that is passed onto the decay products is the spin information of the quark. Because the quark is a spin- $\frac{1}{2}$ fermion, Quantum Mechanics (QM) tells us that the particle can be polarized “spin-up” or “spin-down”. For other quarks, this information is lost when the particle hadronizes. Therefore, the top quark provides a new and unique window into the SM, which gives very specific predictions for the spin correlations between the initial state in top production and final state in top decay.

1.2 Feynman Diagrams and Quantum Field Theory

Before we discuss the top process in detail, a few words should be said about how one goes about calculating the various quantities we can measure for a given process in Particle Physics. These methods involve the subject of Quantum Field Theory (QFT) and Feynman Diagrams.

A Feynman Diagram is an oriented graph that represents an interaction. Using the horizontal axis as time, construct a tree with each line or edge representing a particle. When particles collide or decay, put a vertex that connects the edges representing the particles that are interacting. Different symbols are used for different particles: each fermion is represented by a straight line; the electroweak force carriers (γ , W^\pm , Z^0) are represented by wavy lines; gluons are represented by spirals.¹ Each edge is oriented by the following rule: if it is a particle, put an arrow in the positive time direction; if it is an anti-particle, put an arrow in the negative time direction; for force carriers, the orientation is irrelevant. This tree is called the **tree-level Feynman diagram**. Figure 1 is an example of the Feynman diagram of top quark production and decay (including the decays of the W bosons).

In particle physics, you can only observe the initial and the final states of an interaction; i.e.: only particles corresponding the lines that have a free vertex (“external lines”) are directly observed (the green particles in Figure 1). QM tells us that *any* Feynman diagram with the same initial and final states can contribute to the process. Therefore, we can always add loops in our graph, according to the rules of QFT. These new graphs are

¹There are other symbols for other particles, such as the Higgs Boson or Supersymmetric particles, but these are not relevant to this analysis.

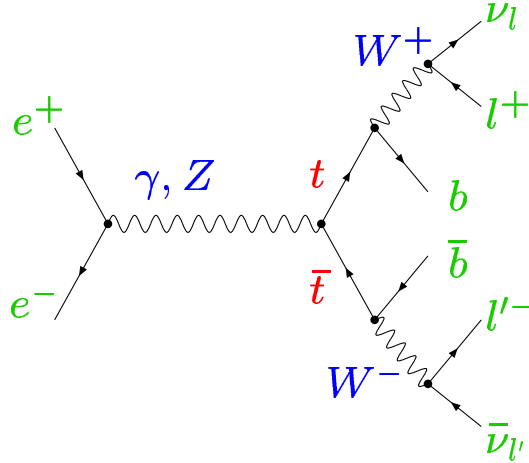


Figure 1: Tree-level Feynman diagram for top production and decay (dilepton event)

called “higher-order diagrams”, and correspond to higher orders in the perturbative QFT expansion. Although these contributions are potentially important in any given process, the tree-level contribution dominates in general, so this thesis will be restricted to a tree-level analysis.

Feynman diagrams are more than an artist’s rendition of a particle interaction. Rather, each diagram represents a mathematical expression corresponding to a quantity known as the **quantum (Feynman) amplitude** (\mathcal{M}); it is also sometimes called the **matrix element** for the interaction. For a tree-level diagram, \mathcal{M} is easily calculated by simply reading off the diagram. The total amplitude is given by the sum of all Feynman diagrams corresponding to the particular initial and final states in question. The magnitude-squared of this quantity is related to the differential probability of this particular interaction with initial and final states occurring. Once the matrix element for a given interaction is known, we can take the magnitude-squared and integrate over all allowed momenta of the final state particles, called **Lorentz-invariant phase space**. This final integral will ultimately yield quantities such as the interaction cross section or particle decay width, which can be measured in experiments.

When dealing with relativistic particles, it is convenient to work with 4-vectors. In relativistic kinematics, one considers the 4-momentum:

$$p^\mu = (E; \mathbf{p}) = (E; p_x, p_y, p_z) \quad \mu = 0, 1, 2, 3 \quad (1.1)$$

where E is the particle’s energy and \mathbf{p} is the particle’s momentum. 4-vectors have the nice property that their norms (p^2) are invariant under coordinate transformations. The norm of

the 4-momentum is very special: it is simply the mass of the particle:

$$p^2 = p^\mu p_\mu = E^2 - |\mathbf{p}|^2 = m^2 \quad (1.2)$$

where we are using (and will continue to use throughout this paper) natural units ($c=\hbar=1$). Being the norm of a 4-vector, the mass is a scalar quantity, and can be computed by measuring the energy and momentum of a particle in any reference frame and plugging the results into Equation 1.2.

However, in QFT, things are not so simple. In the classical regime, Equation 1.2 tells the whole story; but in QM, there is a fundamental uncertainty involved. Particles can exist in QFT even though there is not enough energy to produce them, and unstable particles are produced with an intrinsic distribution. When this happens the particles do not have the proper mass, and Equation 1.2 is no longer strictly valid. These particles with improper mass are called **virtual** or **off-shell**; off-shell particles are often denoted with a “*” (e.g.: γ^*). When the particles are created with the proper mass, the particle is said to be **real** or **on-shell**, and Equation 1.2 is valid again. For this reason, this equation is sometimes referred to as the **on-shell condition**.

1.3 Spin Axes

As mentioned earlier, the top quark is a spin- $\frac{1}{2}$ fermion, so it has two polarization states, which we will call “up” (\uparrow) and “down” (\downarrow). There are an infinite number of ways to define these directions; since from QM, we know that we can choose any axis to be our direction of spin. Part of the trick of this study is to choose a direction for the spin so that the final results can be easily interpreted.

Let \mathbf{s} be a unit vector in some direction along which we will quantize the spin, called the **spin axis**. Then we define our particle to be spin-up if the particle’s spin is aligned along \mathbf{s} , and spin-down if it is anti-aligned along \mathbf{s} . We can define a 4-vector in the particle’s rest frame, which we will call the **spin vector**, as follows:

$$s^\mu = (0; \mathbf{s}) \quad s^2 = -1 \quad s^\mu p_\mu = 0 \quad (1.3)$$

where p_μ is the 4-momentum. The spin vector is a 4-vector, so it can be boosted into any reference frame, and the conditions in Equation 1.3 will still be valid.

We define a “generic spin basis” for the top quark by dictating the angle \mathbf{s} makes with \mathbf{p} . This angle is sufficient for defining a direction for the spin of the quark. By making various choices for this angle, we can see how our results become more or less pronounced.

1.4 Plan

In this thesis, we will be considering the following interactions:

$$e^+e^- \rightarrow (\gamma^*, Z^{0*}) \rightarrow t\bar{t} \rightarrow W^+bW^-\bar{b} \rightarrow [l^+\nu]b[l^-\bar{\nu}]\bar{b} \quad (1.4)$$

$$e^+e^- \rightarrow (\gamma^*, Z^{0*}) \rightarrow t\bar{t} \rightarrow W^+bW^-\bar{b} \rightarrow [l^+\nu]b[q\bar{q}]\bar{b} \quad (1.5)$$

where the brackets in the final state are to emphasize that the leptons or quarks are the daughter particles of the W boson. Specifically, we are looking at the spin correlations between the initial state electron/positron and the final state leptons or quarks coming from the W boson. We will not be considering any W boson helicity issues. The Feynman diagram for interaction 1.4 is given by Figure 1; for interaction 1.5, simply replace the l^-, ν by q, \bar{q}' . Equation 1.4 is called a **dilepton event**, and Equation 1.5 is called a **lepton+jets** event (jets refer to the quarks that come from the W boson decay). Although there are no e^+e^- colliders that can produce top quarks at this time, the Next Linear Collider (NLC), currently in the pre-planning stage, will be able to realize these interactions.

In Chapter 2, the calculations involved are presented and discussed and the necessary information about the spin axes is derived. In Chapter 3, the results from the Monte Carlo generator are shown. Finally, in Chapter 4 we draw conclusions and briefly discuss future prospects.

2 The Calculation

In this section, we derive all of the necessary information used in the Monte Carlo computer program that calculates the correlations. We present the matrix element for the production and decay of a $t\bar{t}$ pair in e^+e^- collisions, and the corresponding cross section. We will then discuss the notion of a *spin basis*, extending the previous ideas from the last section, and present three choices that will be considered in this paper.

A very important part of this analysis was constructing spinors for the top quarks. We will briefly discuss what went into this construction and give the end result. The other key calculation that we needed to perform was to reconstruct the top quark 4-momentum from the final state particles observed. We do this in the case of dilepton events and lepton+jets events. Once all of this information is calculated and coded into the program, the Monte Carlo can be run and results can be realized. These results will be presented in the next chapter.

2.1 Matrix Element and Cross Section

The process under consideration is:

$$e^+e^- \rightarrow (\gamma^*, Z^{0*}) \rightarrow t\bar{t} \rightarrow W^+bW^-\bar{b} \quad (2.1)$$

where the W bosons can decay either leptonically or hadronically. If both decay leptonically, it is called a **dilepton event**; when only one decays leptonically, it is a **lepton+jets (1+jets) event**. In either case, the matrix element for the interaction looks the same (modulo an extra overall factor associated with the quark color, or QCD charge); it is given by:

$$\begin{aligned}
\mathcal{M} &= \frac{1}{64} i e^2 g_w^4 V_{tb}^2 \frac{1}{(p_{W^+}^2 - m_W^2 + i m_W \Gamma_W)} \frac{1}{(p_{W^-}^2 - m_W^2 + i m_W \Gamma_W)} \\
&\times [\bar{u}(\mathbf{b}) \gamma^\alpha (1 - \gamma^5) u(\mathbf{t})] \mathcal{P}(s; \gamma, Z^0) [\bar{v}(\bar{\mathbf{t}}) \gamma^\beta (1 - \gamma^5) v(\bar{\mathbf{b}})] \\
&\times [\bar{u}(\mathbf{I}^-) \gamma_\beta (1 - \gamma_5) v(\bar{\nu})] [\bar{u}(\nu) \gamma_\alpha (1 - \gamma_5) v(\mathbf{I}^+)] \tag{2.2}
\end{aligned}$$

where

$$\begin{aligned}
\mathcal{P}(s; \gamma, Z^0) &= -\frac{Q_t}{s} [\bar{v}_e(\bar{\mathbf{q}}) \gamma^\mu u_e(\mathbf{q})] \gamma_\mu \\
&+ \frac{\csc^2 2\theta_W}{s - M_Z^2 + i M_Z \Gamma_Z} [\bar{v}_e(\bar{\mathbf{q}}) \gamma^\mu (c_V^e - c_A^e \gamma^5) u_e(\mathbf{q}) \gamma_\mu (c_V^t - c_A^t \gamma_5)] \tag{2.3}
\end{aligned}$$

This amplitude is for the on-shell (anti-)top quark, which we will consider in this paper, so the amplitude in Equation 2.2 has the factorized form:

$$\mathcal{M}_{tot} = \mathcal{M}(e^+ e^- \rightarrow t \bar{t}) \mathcal{M}(t \rightarrow W^+ b) \mathcal{M}(\bar{t} \rightarrow W^- \bar{b}) \tag{2.4}$$

We will use this expression in our analysis.

Once we have the amplitude, calculating the cross section for the interaction is a relatively straight-forward task. From Fermi's Golden Rule, the differential cross section is given by the amplitude squared multiplied by some initial flux and a density of states, which is supplied by Lorentz-Invariant Phase Space (LIPS) (see, for example [2]):

$$d\sigma = \frac{1}{2s} |\mathcal{M}|^2 d\mathcal{L} \tag{2.5}$$

$$d\mathcal{L} = \prod_{j=1}^{N_f} \frac{d^3 \mathbf{p}_j}{2E_j} (2\pi)^{4-3N_f} \delta^{(4)} \left(\sum_f p_f - \sum_i p_i \right) \tag{2.6}$$

where s , called the *Mandelstam invariant*, is the square of the center-of-mass (CM) energy, and N_f is the number of particles in the final state (in our case, $N_f = 6$). Our program calculates this amplitude, squares it and integrates it numerically, generating phase space using Monte Carlo techniques.

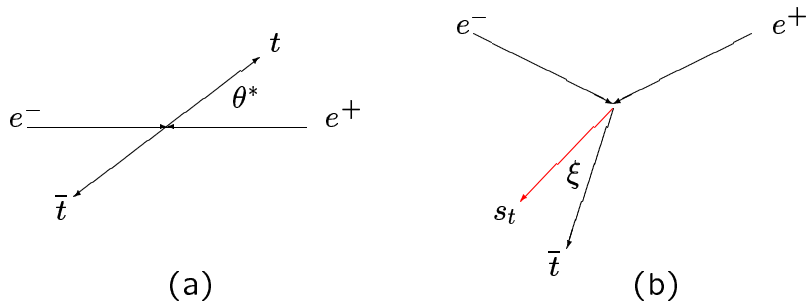


Figure 2: (a) Top quark production in e^+e^- collisions in the CM frame. (b) Generic spin basis: ξ is the angle \mathbf{s}_t makes with the \bar{t} momentum in the top rest frame.

2.2 Spin Bases

Before we develop the details of the calculation, it is important to review the concept of a spin basis. All of the particles involved in this interaction have spin. The quarks and leptons have spin-1/2, and the W , γ and Z^0 bosons each have spin-1. We wish to have a concrete way of talking about the top quark's spin. In order to do this, we need to define a spin axis, which tells us the direction of spin, and a rest frame, since helicity is not Lorentz-invariant.

Figure 2(a) shows the top production mechanism in e^+e^- collisions in the Center-of-Mass (CM) frame. We will use the top quark's rest frame to define the spin axis. There is no formal reason why we cannot choose any direction for the spin axis, but there are a few “natural” choices for a direction; they are discussed here.

In each case, we are defining a generic spin basis, as described by Figure 2(b), which shows the momentum of the e^+ , e^- , \bar{t} in the top quark's rest frame. All of these bases are discussed in much more detail in [3].

2.2.1 Helicity Basis

Perhaps the most natural choice of bases is the Helicity Basis, where we define the spin axis along the direction of the \bar{t} momentum. Since the top and antitop quarks leave the interaction site back-to-back because of conservation of momentum in a head-on e^+e^- collision, this basis defines the top spin to be aligned (or antialigned) with its direction of motion.

Although this is arguably the most natural definition for spin, we will see below that it is not the best axis to use, especially at energies close to the $t\bar{t}$ threshold ($\sqrt{s} \sim 400$ GeV). This will be discussed in the results section.

2.2.2 Beamline Basis

The other natural direction to chose for the spin axis is along the initial electron or positron beam. In this case, define the spin axis to be along the direction of the positron's momentum in the top rest frame.² In the program, we boost the positron's momentum into the top rest frame, and use the new vector as our spin axis. It turns out that this direction does show stronger correlations than the Helicity basis, as will be seen from the results.

2.2.3 Off-Diagonal Basis

The off-diagonal spin axis originally from [4] appears to be much less natural than the other two cases. Looking at the analytic solutions to the cross section, it was found that you can cleverly define your spin axis such that contributions from like $t\bar{t}$ helicities vanish. The source of this convenience comes from the top quark's extremely large mass, rendering the Z^0 width negligible.

There is no intuitive direction (such as one of the particle momenta) that we can use to define the spin axis for the off-diagonal basis. Instead, we turn to the analytic result of [3]. From these results, one can see that there is a way to define the direction of the spin axis (i.e.: the angle ξ ; see Figure 2(b)) so that like top helicity contributions vanish in the differential cross section. The equations for this angle are given by:

$$\tan \xi(e_L^- e^+) = \frac{(f_{LL} + f_{LR})\sqrt{1 - \beta^2} \sin \theta^*}{f_{LL}(\cos \theta^* + \beta) + f_{LR}(\cos \theta^* - \beta)} \quad (2.7)$$

$$\tan \xi(e_R^- e^+) = \frac{(f_{RL} + f_{RR})\sqrt{1 - \beta^2} \sin \theta^*}{f_{RL}(\cos \theta^* + \beta) + f_{RR}(\cos \theta^* - \beta)} \quad (2.8)$$

where the f_{IJ} are the various γ and Z^0 couplings:

$$f_{IJ} = -\frac{2}{3} + Q_Z^I Q_Z^J \csc^2 \theta_W \frac{s}{s - M_Z^2 + iM_Z \Gamma_Z} \quad (2.9)$$

and the Q_Z^I are functions of the Weinberg angle θ_W .

²For the antitop spin correlations, we chose the electron's momentum in the antitop rest frame.

2.3 Spinor Construction

2.3.1 Spinors and the Spinor Helicity Method

Spin-1/2 fermions can be described by spinors that obey the Dirac Equation:

$$(\not{\mathbf{p}} - m)u_s(\mathbf{p}) = 0 \quad (2.10)$$

$$\bar{u}_s(\mathbf{p})(\not{\mathbf{p}} + m) = 0 \quad (2.11)$$

$$\sum_{s=\pm} u_s(\mathbf{p})\bar{u}_s(\mathbf{p}) = (\not{\mathbf{p}} \pm m) \quad (2.12)$$

Equation 2.12 is called the *completeness relation* and must be satisfied in order for u (\bar{u}) to be a spinor. The sign on the right hand side is determined by whether u describes a particle ($-$) or antiparticle ($+$).

Normally, when computing a cross section, one sums and squares the amplitudes analytically and uses Equation 2.5. For a complicated amplitude such as the one in Equation 2.2, this can become very cumbersome. Moreover, the result translated into computer code for numerical computation can be very CPU-intensive. However, if the (complex) amplitudes themselves can be computed numerically, the calculations would be greatly simplified and much more efficient. This was first noticed by [5], and led them to develop a method of calculating amplitudes, commonly known as the **Spinor Helicity Method**. We will be employing their ideas.

Results derived independently by [4, 5] have shown how one can construct massive spinors from massless ones. In this section, the basic ideas behind this construction are discussed. Details of the calculations can be found in [5].

Begin with a massless spinor $u_s(k)$ that satisfies Equation 2.10 (with $m \equiv 0$). We also chose two 4-vectors (k_0, k_1) with the following properties:

$$k_0^2 = 0 \quad k_1^2 = -1 \quad k_0 \cdot k_1 = 0 \quad (2.13)$$

Now make the following definitions for the spinors:

$$u_-(k_0)\bar{u}_-(k_0) = \frac{1}{2}(1 - \gamma^5) \not{k}_0 \quad (2.14)$$

$$u_+(k_0) = \not{k}_1 u_-(k_0) \quad (2.15)$$

One can show that these spinors satisfy Equation 2.12 and are therefore valid spinors for massless particles.

To construct spinors for massive particles (e.g.: the top quark), we do the following trick. For a particle of mass m , spin s and 4-momentum q , we can express a spinor that describes the particle in terms of some lightlike (massless) 4-vector k :

$$u(q, s) = (\not{q} + m)u_-(k)/\sqrt{2q \cdot k} \quad (2.16)$$

Now decompose the particle's 4-momentum into two massless 4-vectors p_1, p_2 so that $p_1 + p_2 = q$ and $p_1^2 = p_2^2 = 0$. Now choose $k = p_2$:

$$u(q, s) = \frac{1}{m}(\not{p}_1 + \not{p}_2 + m)u_-(p_2) \quad (2.17)$$

Finally, we can simplify this expression, and repeat the process for both helicities and for particles (u) and antiparticles (v) to get:

$$u(q, +s) = \alpha u_+(p_1) + u_-(p_2) \quad (2.18)$$

$$u(q, -s) = \beta u_-(p_1) + u_+(p_2) \quad (2.19)$$

$$v(q, +s) = \alpha u_+(p_1) - u_-(p_2) \quad (2.20)$$

$$v(q, -s) = \beta u_-(p_1) - u_+(p_2) \quad (2.21)$$

where

$$\alpha = \frac{\bar{u}_+(p_1)u_-(p_2)}{m} \quad \beta = \frac{\bar{u}_-(p_1)u_+(p_2)}{m} \quad (2.22)$$

are complex phases. Using this technique, the top quark spinors can be correctly expressed in terms of massless spinors. It is important to notice that most of our input was somewhat arbitrary: the massless momenta needed only to add up to the total massive quark

momentum q , and s needed only to satisfy Equation 1.3. This freedom is compensated for in Equations 2.18-2.21 by the phases α and β . We are free to choose any vectors that would make the calculations easier, as long as we could calculate the changes in these phases. This was a key point that made the calculation doable without resorting to calculating any traces, which is the standard approach to QFT calculations.

2.3.2 Rotating the Spinors

Now that we have a powerful way of constructing the spinors for the top quark that appear in the amplitude of Equation 2.2, we may calculate the amplitude for the cross section. In order to measure the spin correlations consistently, we must perform a rotation on the spinors defined above. This change corresponds to picking a new massless vector k_1 . As stated in the previous paragraph, we are allowed to do this, as long as we are careful to keep track of any new phases that appear. In the rest of this section, we will derive an expression for this new phase.

A word on notation: the phase calculated in this section is not the same as the phases α and β mentioned above; α and β are already calculated by the program from Equation 2.22. This new phase we are calculating here comes from the SU(2) spinor rotation (see, for example, [6]).

We begin searching for new spinors by performing a standard SU(2) rotation on the old ones:

$$\begin{pmatrix} u'_+ \\ u'_- \end{pmatrix} = \begin{pmatrix} a & b \\ -b & a \end{pmatrix} \begin{pmatrix} u_+ \\ u_- \end{pmatrix} \quad (2.23)$$

where a and b are complex, and $|a|^2 + |b|^2 = 1$. Our program uses a spin vector:

$$s = \frac{1}{m}p - \frac{m}{pk_0}k_0, \quad k_0 = (1; 1, 0, 0) \quad (2.24)$$

where k_0 is our massless 4-vector that we used in constructing our massless spinors (see Equation 2.13). Notice that Equation 2.24 obeys all conditions in Equation 1.3 and is therefore a valid spin vector. After some manipulation, and using the completeness condition (Equation 2.12), we can construct a new spin vector from the old one:

$$s' = (a^2 - b^2)s + 2ab(k_1 - \frac{pk_1}{pk_0}k_0) = \gamma(\beta; \mathbf{n}) \quad (2.25)$$

where γ is the Lorentz factor and $\mathbf{n} = \frac{\mathbf{p}}{|\mathbf{p}|}$. Now we must choose a vector for k_1 that will satisfy Equation 2.13. Try:

$$k_1 = \frac{1}{\sqrt{n_y^2 + n_z^2}}(0; 0, n_y, n_z) \quad (2.26)$$

Plugging this value for k_1 in Equation 2.25 and grouping terms, we derive a constraint on a and b to get, after a lot of arduous algebra:

$$ab = \frac{m}{2pk_0} \left\{ \left[\frac{pk_1}{pk_0} + \frac{n_z}{\sqrt{n_y^2 + n_z^2}} \right]^2 + \frac{m^2}{(pk_0)^2} \right\}^{-\frac{1}{2}} \quad (2.27)$$

Given this constraint, along with the unimodular condition $|a|^2 + |b|^2 = 1$, we have enough information to solve for a and b , up to a sign and a phase difference.

First let us discuss the sign convention. In this analysis, s' must be positive definite. A sufficient condition for this to occur is for $s'^0 > 0$. Also notice that Equation 2.23 is invariant under the transformation $(a, b) \rightarrow (-b, a)$, but by Equation 2.25 under this same transformation, $s' \rightarrow -s'$. Therefore this transformation allows us to set a sign convention: if $s'^0 > 0$, leave everything alone, but if $s'^0 < 0$, perform the transformation $(a, b) \rightarrow (-b, a)$. This fixes the sign of a and b in our program.

The relative phase is slightly more complicated. As mentioned earlier, this phase comes in because we have chosen a k_1 that made the calculation easier, but is not consistent with the rest of the program. The problem does not affect our expressions for $u_+(\mathbf{p})$ or $v_-(\mathbf{p})$, because they are derived from $u_-(k_0)$, which has no dependence on k_1 (c.f. Equation 2.14). However, our spinors $u_-(\mathbf{p})$ and $v_+(\mathbf{p})$ do depend on k_1 , since they are constructed from $u_+(k_0)$ (cf Equation 2.15). To emphasize this dependence on k_1 , we will refer to these last three spinors as $u_+^{k_1}(k_0)$, $u_-^{k_1}(\mathbf{p})$ and $v_+^{k_1}(\mathbf{p})$. Since the new choice of k_1 differs from the rest of the program, everything dependent on it will pick up a phase. So we must worry about the phase of these two spinors.

Calculating this phase is not very difficult. Using the conditions of Equation 2.13 along with some basic QFT, we obtain for the massless spinor $u_+^{k_1}(k_0)$:

$$u_+^{k_1}(k_0) = e^{i\delta} u_+^0(k_0), \quad e^{i\delta} = \frac{n_y - in_z}{\sqrt{n_y^2 + n_z^2}} \quad (2.28)$$

Combining all of this with the results already mentioned, Equation 2.23 has the new form for the top and antitop respectively (with a and b real):

$$\begin{pmatrix} u'_+ \\ u'_- \end{pmatrix} = \begin{pmatrix} a & be^{i\delta} \\ -b & ae^{i\delta} \end{pmatrix} \begin{pmatrix} u_+ \\ u_-^{k_1} \end{pmatrix} \quad \begin{pmatrix} v'_+ \\ v'_- \end{pmatrix} = \begin{pmatrix} ae^{i\delta} & b \\ -be^{i\delta} & a \end{pmatrix} \begin{pmatrix} v_+^{k_1} \\ v_- \end{pmatrix} \quad (2.29)$$

2.4 Top Momentum Reconstruction

Throughout this analysis, a key quantity we need is the top quark's momentum.³ In theory, this is not a problem. The Monte Carlo generates the top momentum, so all we need to do is retrieve it. However, things do not work so easily in the experiment, where you can only see what particles come out in the final state. In such a case, it is necessary to reconstruct the top momentum from the final state using conservation laws and mass constraints. This reconstruction can have some noticeable effects on the results. For example, it turns out that the reconstruction may give more than one solution for the top momentum, and there may not be enough constraints to eliminate one of them. In such cases, we must take both solutions as physical. This can have the effect of “watering down” our data, and one may want to know how serious an effect this might have.

In this thesis, we reconstruct the top momentum, and see if there is any way to eliminate multiple solutions. We assume, like the experimentalists, that we can only see the final state: jets, leptons, and missing energy and momentum (from the neutrinos); notice that we do *not* assume that we know which jet is which. However, we do ignore hadronization effects, and perform all calculations at the parton level. Throughout this section, we will be referring to Figure 3, which shows the particles and their momenta.

Consider $t \rightarrow W^+b$. Simple conservation of momentum gives $\mathbf{p}_t = \mathbf{p}_{W^+} + \mathbf{p}_b$. Move \mathbf{p}_b to the other side of the equation and square both sides to get an equation for $\cos\theta_{tb}$ in terms of the magnitude of the three momenta:

³In an e^+e^- machine, the $t\bar{t}$ come out back-to-back by conservation of momentum, so if you know the top momentum, you get the antitop momentum for free!

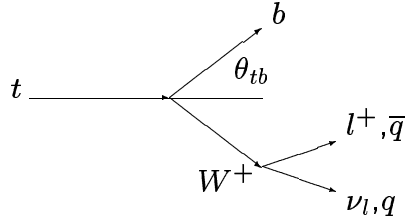


Figure 3: Top quark decay to a b quark and a W^+ boson.

$$\cos \theta_{tb} = -\frac{|\mathbf{p}_{W^+}|^2 - |\mathbf{p}_t|^2 - |\mathbf{p}_b|^2}{2|\mathbf{p}_t||\mathbf{p}_b|} = \frac{E_b E_t - \frac{1}{2}(m_t^2 - m_b^2 - m_W^2)}{|\mathbf{p}_t||\mathbf{p}_b|} \quad (2.30)$$

A similar equation holds for $\cos \theta_{t\bar{b}}$, but with a minus sign (since the top and antitop are back to back). This last point is crucial to being able to tell which is the bottom quark and which is the antibottom quark.

Now notice that in the interaction, the total 4-momentum is given by $q_0 = (\sqrt{s}; \mathbf{0})$. Furthermore, knowing that the $t\bar{t}$ came out back-to-back implies $E_t = E_{\bar{t}} = \frac{\sqrt{s}}{2}$. Now use the fact that the top quark is assumed to be on-shell to get $|\mathbf{p}_t|$ from the on-shell condition (Equation 1.2). Notice that $|\mathbf{p}_t| = |\mathbf{p}_{\bar{t}}|$.

E_b and $|\mathbf{p}_b|$ are known because they can be measured. Then using the same conditions mentioned above, along with the on-shell condition for the W boson, we can find $|\mathbf{p}_{W^+}|$. Given this information, the angle $\cos \theta_{tb}$ is now known from Equation 2.30.

Now we can construct three equations in terms of the three components of the top momenta: two from $\mathbf{p}_t \cdot \mathbf{p}_b$ and $\mathbf{p}_{\bar{t}} \cdot \mathbf{p}_{\bar{b}}$ (which is why we needed to know $\cos \theta_{tb}$), and one from the on-shell condition. This third equation is a quadratic, so we end up with two independent solutions for the top momentum. Finally the antitop momentum is given by the negative of these solutions.

We have reconstructed the top (and antitop) momenta; however, there are two possible solutions. The next logical question is: can we eliminate one of the solutions? We consider the dilepton and l +jets channels separately.

2.4.1 Dilepton Events

One can do the same thing done above for the equation $\mathbf{p}_{W^+} = \mathbf{p}_{l^+} + \mathbf{p}_\nu$, along with the condition that we can measure the total missing energy and momentum, $\cancel{E}, \cancel{\mathbf{p}}$. Employing the last condition that $p_\nu + p_{\bar{\nu}} = (\cancel{E}; \cancel{\mathbf{p}})$, where the p_i are the neutrino 4-momentum and $p_i^2 = 0$, the quadratic mass constraints can be reduced to a single linear equation, and there are now six linear equations for six unknowns (each component of the momentum for each neutrino). This is enough to solve for the neutrino momenta exactly!

Once we know the neutrino momenta, eliminating one of the solutions for the top momentum is trivial: only one of the two solutions for the top momentum will be consistent with the neutrino momenta. This constraint will always pick the correct solution in our program. As a check, we compared our reconstructed momentum with the computer's generated momentum, and each time it came up with the right answer.

Finally, we wish to remove the assumption that we know which b-quark is which. However, just notice that switching the bottom and the antibottom quarks is equivalent to introducing a minus sign in Equation 2.30, as mentioned earlier. Once again, it is an easy check to see whether the minus sign belongs there by comparing your solutions to the reconstructed neutrino momenta. Therefore, we need not know which quark is which in order to perform this reconstruction. The *only* assumption that was necessary was to assume all of the particles were on-shell.

2.4.2 1+jets Events

In 1+jets events, there are four jets, one lepton and missing energy and momentum (see Figure 3 with $W^+ \rightarrow q\bar{q}$). We now have to worry about knowing which jets belong to the b quarks, and which came from the W boson. One way to do this is to tag the jets.⁴ Three possibilities are left open: we can tag two b-jets, one b-jet or no b-jets. If we can tag two b-jets, the problem is equivalent to the dilepton case, and we need not discuss this case any further.

For the other cases of one and no tagged b-jets, the problem is slightly less trivial. In the former case, there is one jet that is identified as a b quark, and three jets are unidentified.

⁴In experiments, we can identify a b-jet by the presence of a muon in the jet, for example.

However, there is an additional constraint that we can use. Because two of the jets must be decay products of a W boson, we can consider the invariant mass of any two unidentified jets:

$$m_{ij}^2 \equiv (p_i + p_j)^2, \quad i, j = 1, 2, 3 \quad (2.31)$$

where the p_i are the 4-momentum of the jets in question. One of these invariant masses m_{ij} must be equal to m_W ; then p_i and p_j are the two jets from the W boson, and the remaining jet is the other b-jet. Now that we know the bottom and antibottom momenta, we can proceed with the previous algorithm to calculate the top momentum.

A word of caution: the previous statement assumes that we have a unique solution. In a real experiment, these jets have a momentum spread to them, and this error is a primary concern to the measurement. Our program does not treat this momentum smearing, since all of the calculations are at the parton level. However, it is important to see how this spread will affect our jet identification. Therefore, we not only accept the two jets with an invariant mass equal to m_W , but any pair of jets with invariant mass within some error of m_W is allowed, since they could be misidentified in an experiment. One chief question to ask is how to quantify this condition. This issue will be addressed next chapter.

Once the algorithm to handle single tagged b-jet events is coded, handling no tagged b-jet events is a simple extension. The only difference is that there are six jet-pair invariant masses to consider instead of three. One of these pairs will have an invariant mass equal to m_W , and the remaining two jets are the b-jets. The same argument of jet-momentum smearing still applies.

We have shown the Feynman amplitude for the process of top production and decay in e^+e^- collisions, and have constructed three spin bases for the analysis. We have discussed how to treat the spinors that appear in the matrix element. Finally we have discussed how to bring this analysis closer to life by reconstructing the top quark momentum from the final state particles rather than using the generated top momentum, and how this reconstruction introduces a systematic uncertainty in our results. In the next chapter, we will present the results of these calculations, and discuss the cuts for jet identification in 1+jets events.

3 Numerical Results

“We are at last in possession of a full deck, and we know the rules of the game– it’s time to deal!” *–D.J.Griffiths, Introduction to Electrodynamics, 3rd Edition*

In the previous chapter, all of the necessary information was derived and presented. Now at last we are in a position to present results. All of these results were done under the assumption that the top quark (and the top antiquark) were on-shell. We always use our reconstructed momenta, and if there is no way to eliminate erroneous solutions, we use both of them. We consider left and right polarized electron beams in the initial state, with an unpolarized positron. In the l+jets case, without any loss of generality we let the W^- decay hadronically, so we always have a l^+ in the final state. We will consider the spin correlations between the initial electron and this final l^+ in all three bases mentioned in the previous chapter. Similar correlations can be drawn with other particles, but the correlations are generally strongest with the l^+ , and the momentum is the most cleanly measured (see [3]). All of the plots are included at the end of the chapter.

It is a well known general result (see [7]) that the differential branching fraction of a *polarized* top decay has the form:

$$\frac{1}{\Gamma_T} \frac{d\Gamma}{d \cos \chi_i} = \frac{1}{2} [1 + \alpha_i \cos \chi_i] \tag{3.1}$$

where $\cos \chi_i$ is the angle between the top quark spin axis and the momentum of the i^{th} particle in the decay $(b, \bar{b}, q, \bar{q}, l^\pm, \nu)$, and α_i is a constant. In the case of the l^+ correlations, $\alpha_i=1$. After summing over top polarizations, we expect to see an equation similar to Equation 3.1, linear in $\cos \chi$. These plots will be shown for the dilepton and l+jets cases separately. Further, we will consider the results in the l+jets case for each choice of b-quark tagging.

Another interesting fact is that for large β_t ; or equivalently for large \sqrt{s} , the three bases mentioned above become equivalent. To emphasize this fact, we will consider these correlations at $\sqrt{s} = 400$ GeV and 500 GeV. The NLC is currently planned to be constructed for a CM energy of 500 GeV, hence this choice. At 500 GeV, the three bases begin to overlap. We consider 400 GeV since it is close to the $t\bar{t}$ threshold, where the differences in the three bases are most striking. At energies close to 1 TeV, the bases are nearly identical, so we will not discuss this case.

We will also mention something about the reconstructed W momenta in the l+jets case, where there is a systematic uncertainty due to the smearing of the jet momenta. This error manifests itself in the W mass reconstruction. Using this reconstructed W mass is the first step toward allowing the top quark to go off-shell.

3.1 Dilepton Events

Dilepton events are given by the interaction of Equation 1.4. In this case, there are two neutrinos, and one might worry that the problem is overconstrained. Indeed, this is precisely what happens when you do not assume that the top quark is on-shell. In such cases, the standard procedure is to assume a distribution of top masses and construct a likelihood fit. In this analysis, however, the top quark is assumed to be on-shell, and this simplifies the problem substantially.

As mentioned in the previous chapter, knowing that the particles are on-shell is enough to give you a unique solution for each neutrino. Once this solution is known, one of the top quark momentum solutions can be eliminated by a consistency check, and we have a unique and final solution for the top quark momentum, which can be used to construct the spin basis. Consistency checks between reconstructed and generated momenta were performed in the program, and each reconstruction yielded the correct value for the top momentum.

The spin correlations for dilepton events are presented in Figures 4 and 5 for various CM energies. With a unique top momentum, these results are exactly analogous to the results previously calculated analytically by [3]. There is a sign change in the slope when looking at left-polarized versus right-polarized electrons, as expected from these analytic results. Notice that at lower energies, the slope of the Helicity basis correlation is much weaker than

the Beamline or Off-Diagonal bases. Further, notice that the Off-diagonal basis has the strongest variation with $\cos \chi$, justifying the statement that the Off-diagonal basis was the best to see strong correlations close to threshold. Also, as stated above, for higher \sqrt{s} the three bases become equivalent.

3.2 1+jets

3.2.1 Jet Reconstruction

When considering 1+jets events, there are more jets that must be identified. Previously, with only two jets coming from different branches of the decay process, it was reasonable to assume that we can distinguish between the two jets. That assumption is no longer valid.

Although we continue to work at the parton level, an error in our jet distinction can be incorporated by allowing $|m_{ij} - m_W| \leq \delta E$, where δE is the error in jet resolution in the detector, and m_{ij} is given by Equation 2.31. This error is given by an empirical value called the jet resolution:

$$\frac{\delta E_T}{E_T} \sim \frac{f}{\sqrt{E_T}} \quad \text{where} \quad E_T = p^0 \sqrt{\frac{(p^1)^2 + (p^2)^2}{\mathbf{p}^2}} \quad (3.2)$$

where f is some fraction. E_T is called the **transverse energy** of the jet.

The fraction f can only be determined from experience. At the D0 Experiment at Fermilab, f is ideally approximated by 80% [8]. Using this value for f at typical b energies of 87 GeV, one can approximate $\delta E \sim 8$ GeV. This jet resolution is large enough to have some jets overlap, so that several m_{ij} are allowed.

We can minimize this problem somewhat by performing the same consistency check we performed for the dilepton case, and see if any pair of jets is inconsistent with our reconstructed light-quark momenta (which replace the neutrino of the dilepton case, but are still considered massless). Anytime we can chose a jet pair with momentum that is consistent up to 8 GeV, we keep it; anything outside of that, we drop. This has the effect of eliminating many of the solutions, but not all of them: Table 1 give the average number of solutions that pass per event, in both single and no b-jet tagging. This leads to an ambiguity in our results (see below).

At this point, a logical question to ask is: Why not simply do what has been done in the

<i>Number of b-tags</i>	<i>Processed Solutions:Real events</i>
1	1.12:1
0	1.18:1

Table 1: Ratio of averaged allowed solutions per event.

dilepton case, taking advantage of the massless quarks? We can attempt to reconstruct the light-quark momenta, and check for consistency. It turns out that this is not realistic. When the particles come out as jets in the detector, it is very difficult to reconstruct the masses of the original partons. In reality, jets are identified with their original parton by tagging techniques. For example, the b quark decays very rapidly in the detector, so it is more likely to decay to muons via the weak interaction much faster than the light mesons from u or d jets, for example. Experimentalists look for these muons in the jet, and use them to “tag” the b . So, it is better to avoid the technique of directly using the masses of the partons, but rather to compare jet-pair invariant mass with the W boson mass.

3.2.2 W Mass Reconstruction

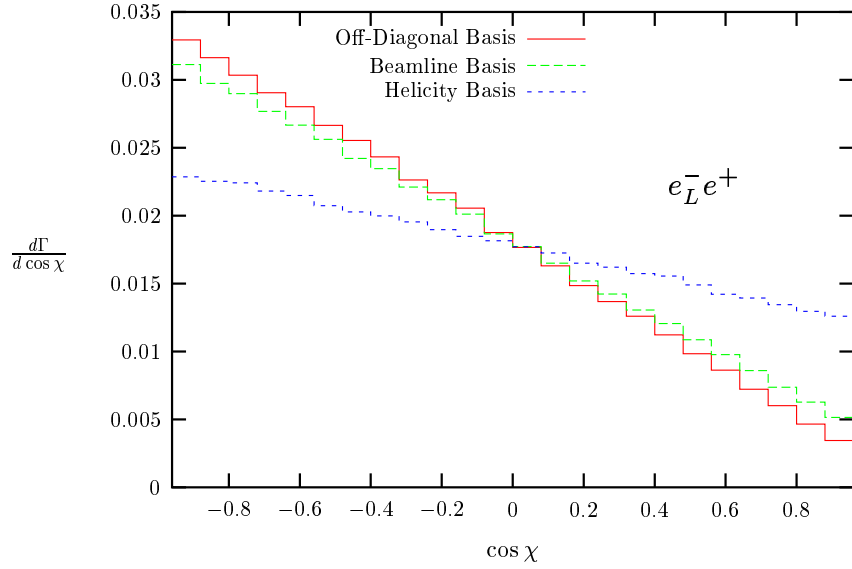
One effective way of determining the effectiveness of the jet identification criterion comes from the W boson itself. Because we have reconstructed the top momentum from jets, we can now ask: How does our error in jet selection affect the mass of the W boson? Realistically, we should always calculate the mass of the W boson from the reconstructed jets, and then use that value when reconstructing the top quark momentum. The error in the jet selection would then become an error in m_W resolution.

The results of this check are shown in Figure 6. Notice that the mass is peaked strongly at the real value (in the program, $m_W = 80.0$ GeV). However, there are some outlying events between 72 GeV and 88 GeV, which were allowed by our treatment of jet resolution. It is these outliers that produce the difference in the l+jets plots versus the dilepton plots (see below).

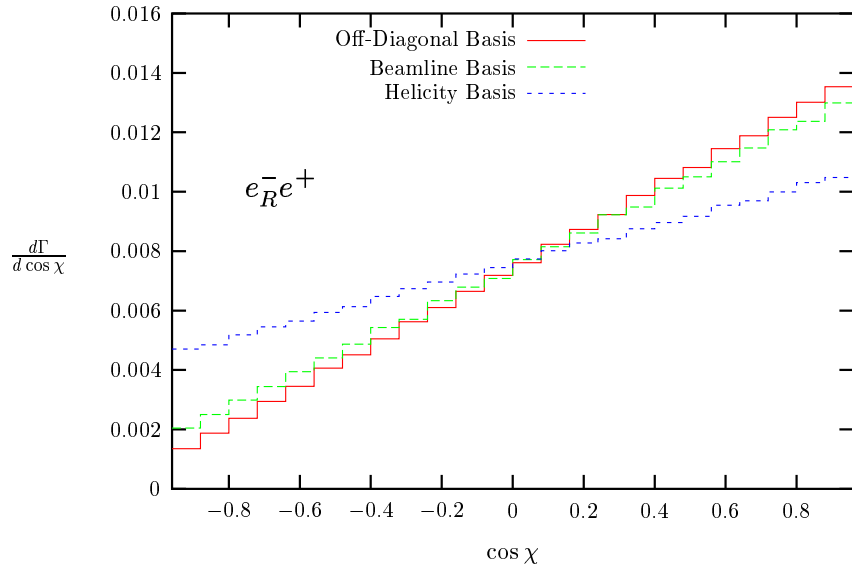
3.2.3 Results for Different b-jet Tagging

The results for l+jets are presented in Figures 7 through 10. The first two figures are for single tagged b-jet events, and the next two figures are for no tagged b-jet events. There

are many similarities between these plots and those for dilepton events, but there are some striking differences. The chief difference is in the large jump for small $\cos\chi$. This deviation is due to the extra events that have polluted our sample (see Table 1). These effects may be important when the experiment is performed.

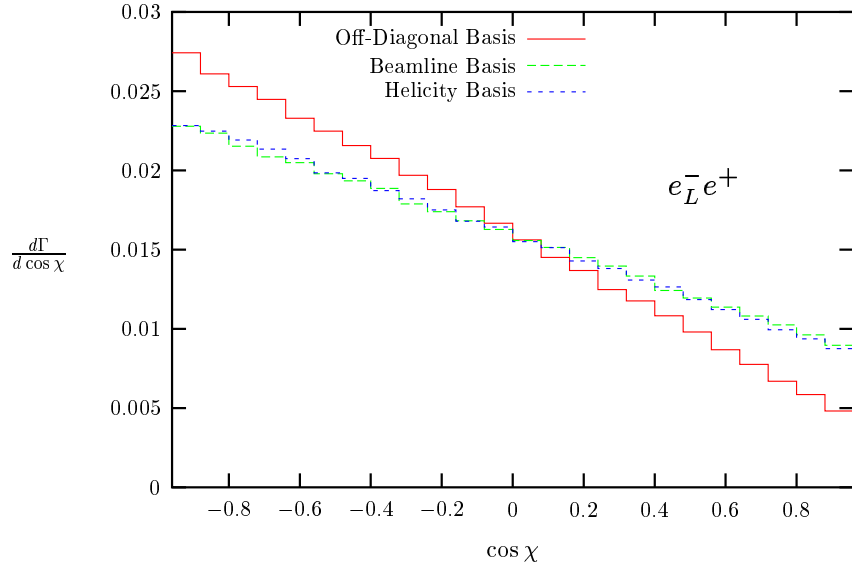


(a)

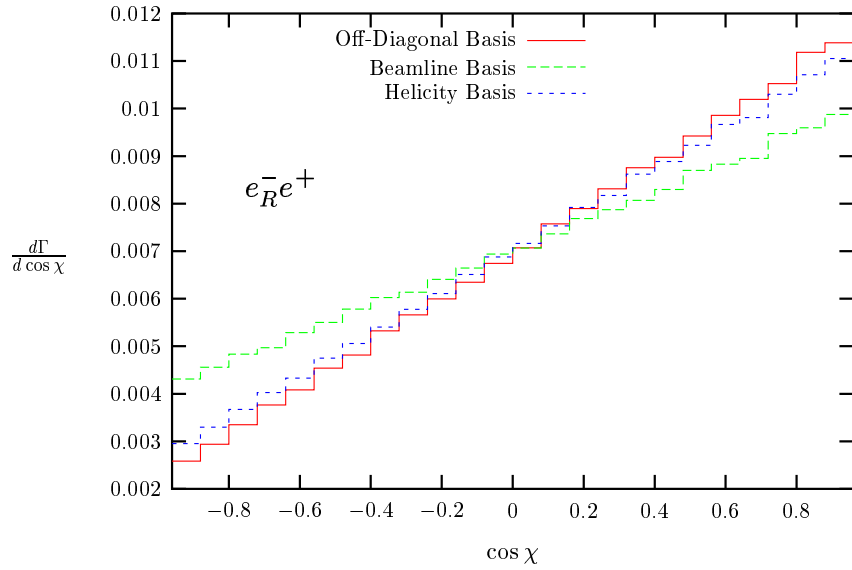


(b)

Figure 4: Reconstructed spin correlations in dilepton events at $\sqrt{s} = 400$ GeV for final state lepton (l^+) and left (a) and right (b) polarized electron beams.

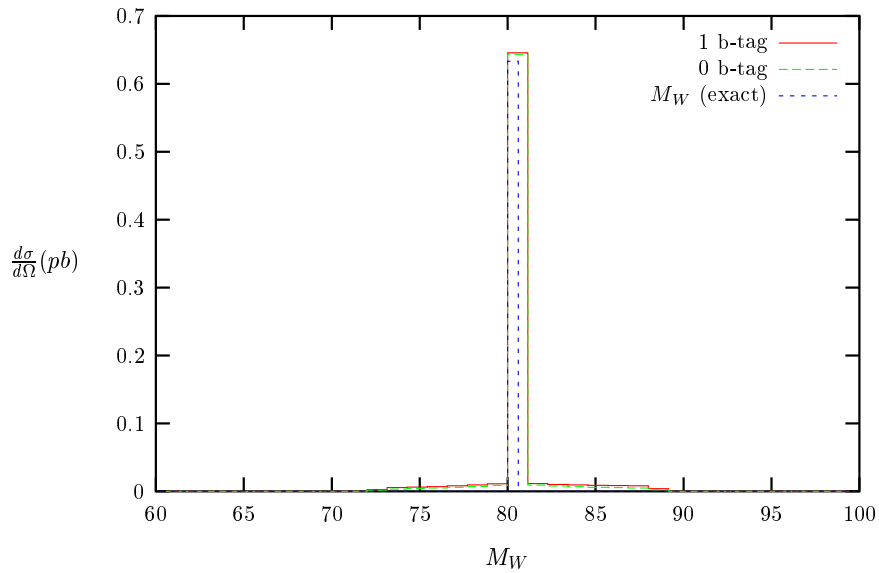


(a)

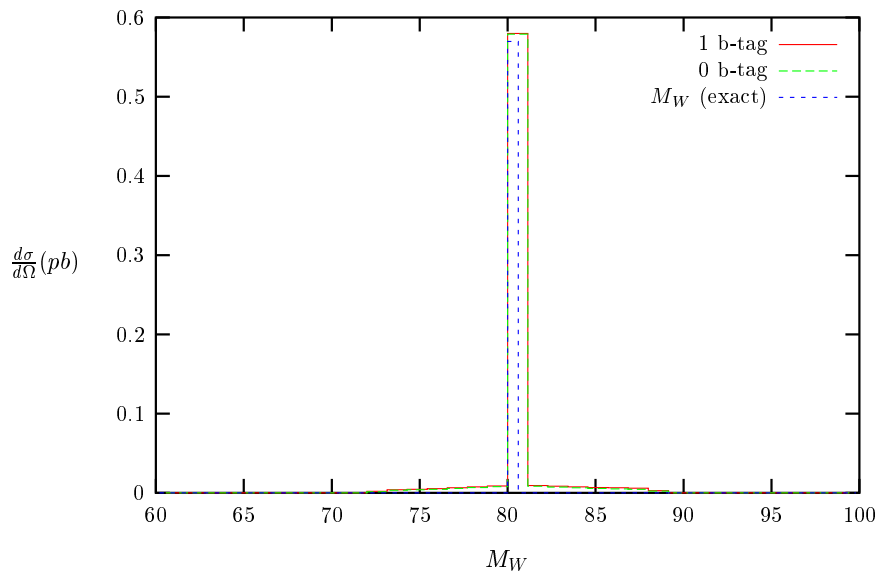


(b)

Figure 5: Reconstructed spin correlations in dilepton events at $\sqrt{s} = 500$ GeV for final state lepton (l^+) and left (a) and right (b) polarized electron beams.

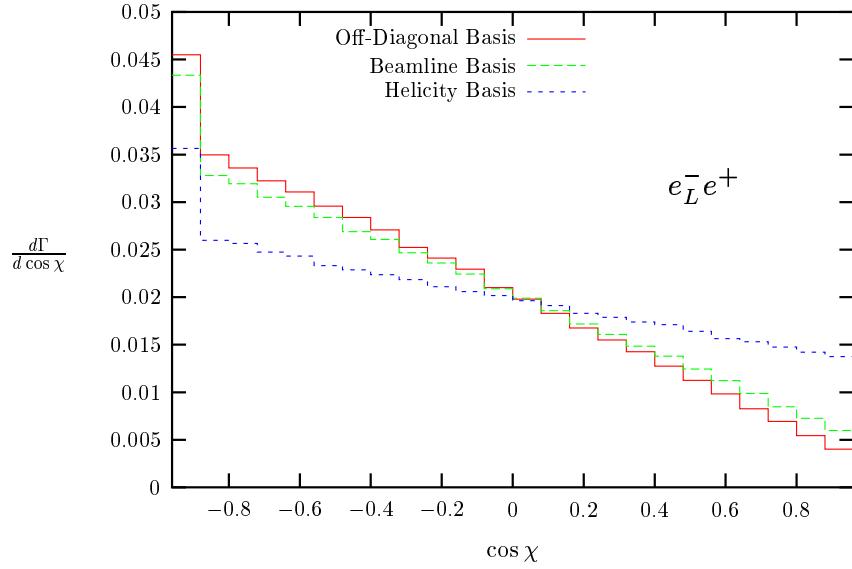


(a)

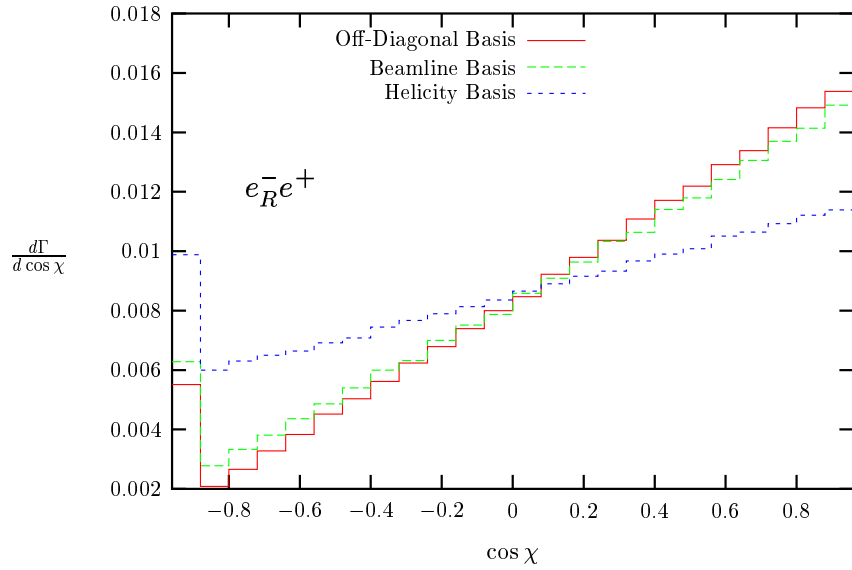


(b)

Figure 6: Reconstructed W boson mass in l+jets events with two (exact), one and no tagged b quarks at $\sqrt{s} = 400$ GeV (a) and $\sqrt{s} = 500$ GeV (b). The program used $M_W = 80.0$ GeV.



(a)



(b)

Figure 7: Reconstructed spin correlations in $l+\text{jets}$ events with a single tagged b quark at $\sqrt{s} = 400$ GeV for final state lepton (l^+) and left (a) and right (b) polarized electron beams.

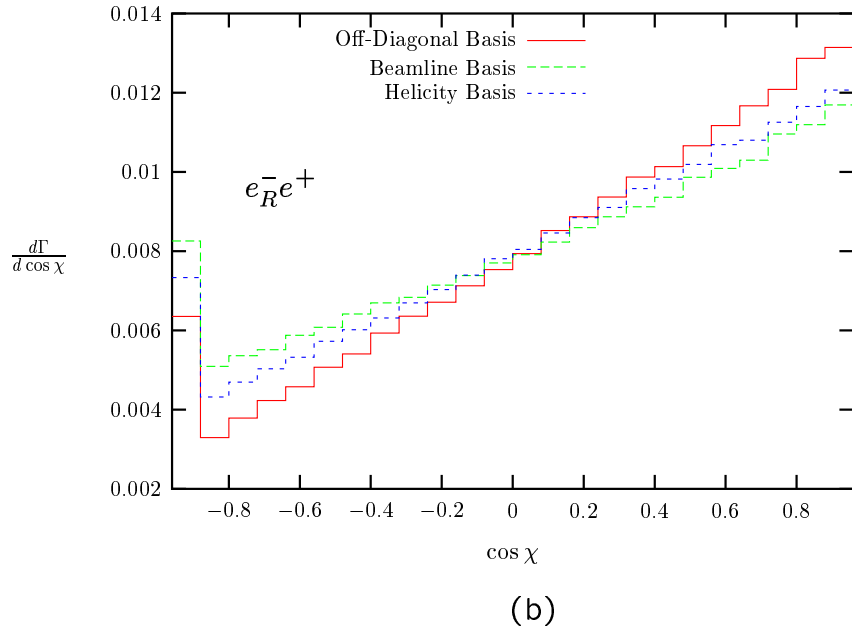
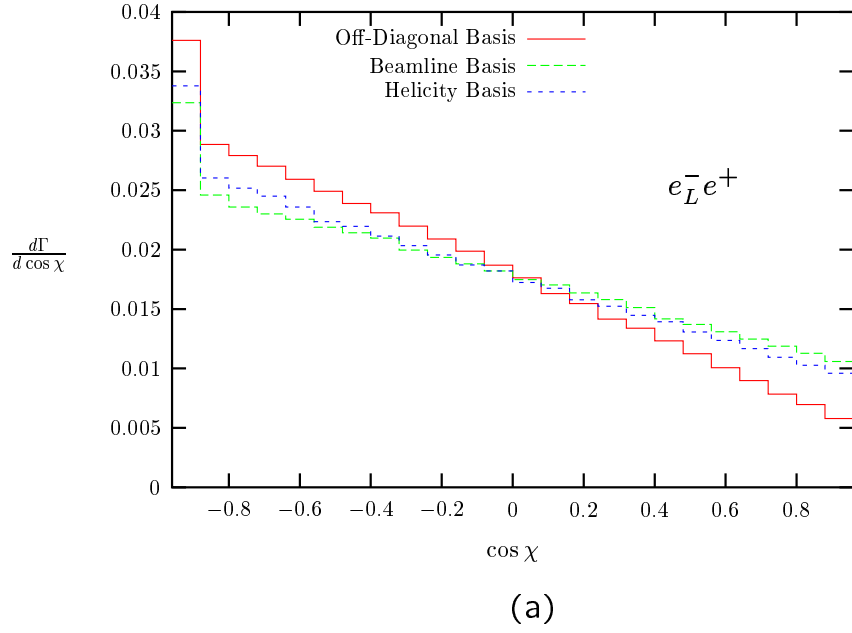
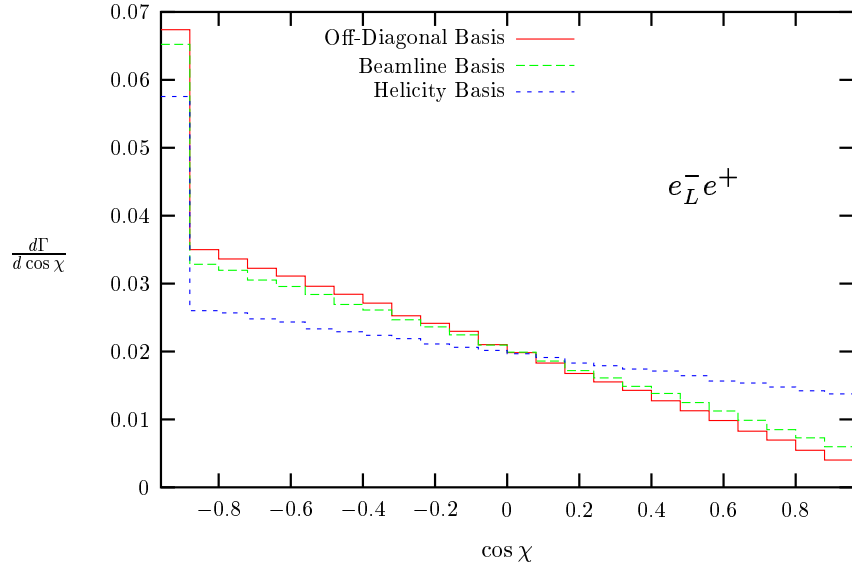
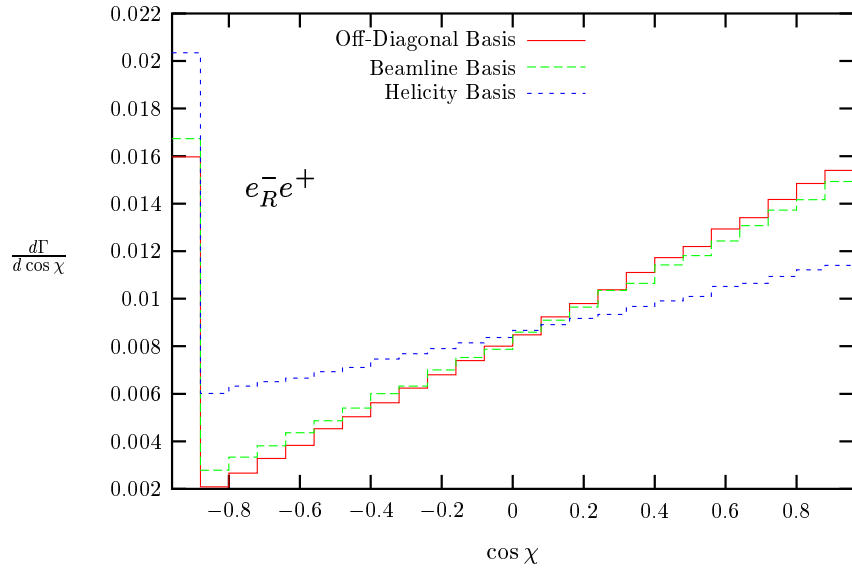


Figure 8: Reconstructed spin correlations in $l+\text{jets}$ events with a single tagged b quark at $\sqrt{s} = 500$ GeV for final state lepton (l^+) and left (a) and right (b) polarized electron beams.

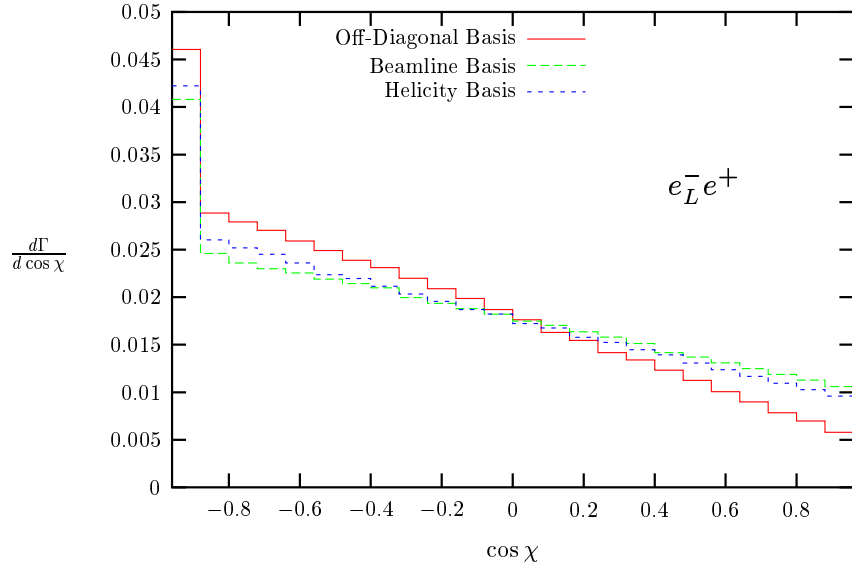


(a)

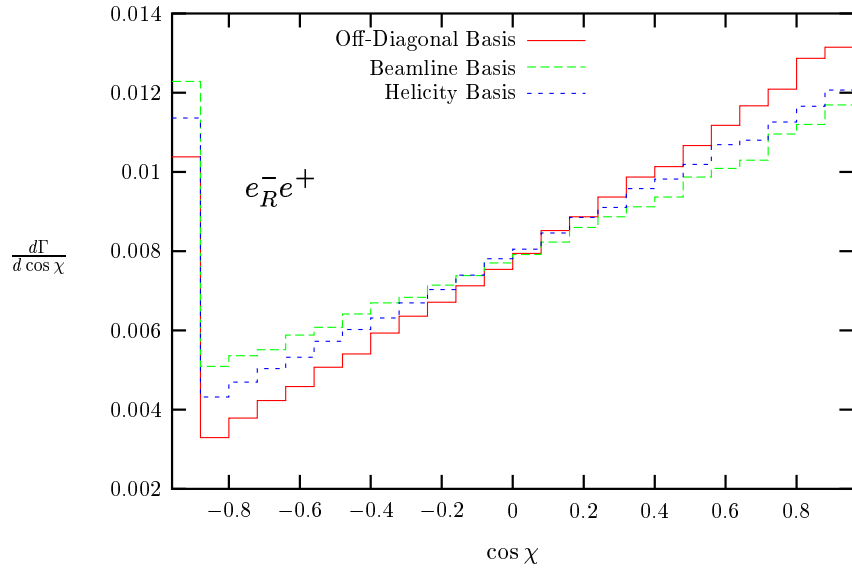


(b)

Figure 9: Reconstructed spin correlations in l^+ jets events with no tagged b quarks at $\sqrt{s} = 400$ GeV for final state lepton (l^+) and left (a) and right (b) polarized electron beams.



(a)



(b)

Figure 10: Reconstructed spin correlations in l +jets events with no tagged b quarks at $\sqrt{s} = 500$ GeV for final state lepton (l^+) and left (a) and right (b) polarized electron beams.

4 Conclusions

The top quark provides particle physicists with a new and unique probe for testing the Standard Model of Particle Physics (SM) and searching for new physics beyond. Its immense mass, and therefore short lifetime, allows the quark to decay before hadronization can occur. Therefore, data such as the spin information are naturally passed onto the daughter particles, and the SM predicts very specific results for such a decay. Calculations involving these spin correlations in e^+e^- collisions have already been performed by [3]. However, in all of the analyses to date, the calculations have used direct analytic methods to solve for the correlations. This is not how these measurements can be done, because no experiment can measure the top momentum directly, due to the extremely short lifetime of the top quark. Therefore, in order to accomplish these measurements, experimentalists need an algorithm for doing these calculations in terms of quantities that can be measured directly, specifically the energy and momenta of the particles in the final state.

This thesis is the first attempt to do this analysis from a more realistic point of view in e^+e^- machines. We started with a program that would calculate the cross sections using the “Spinor Helicity Method” of Kleiss and Stirling. We then performed a reconstruction of the top momentum in terms of the final state particles, for both dilepton and l+jets events. For the l+jets case, we tried to make the problem more realistic by assigning an uncertainty in the jet resolution, which in turn introduces an uncertainty in the the jet identity and therefore W boson mass. Factoring in this uncertainty for the top quark momentum reconstruction is the first step in doing this analysis for off-shell top quarks.

In the process of getting these results, it was found that the theoretically predicted correlations can be obtained for the dilepton events, even after the reconstruction. However, using the error in the jet resolution, we found that we cannot always eliminate the erroneous

solutions in the top quark reconstruction. These results led to a deviation in the predicted correlations in the 1+jets events for small $\cos\chi$. There is a possibility that this deviation can be reduced or even eliminated with more consistency checks similar to the dilepton case; however, we wish to avoid these comparisons, since they are much more difficult to measure in an experiment.

At this point, there are several things we can do to refine this analysis. One idea would be to start looking at an off-shell top quark, and seeing what that would do to our results. Another idea is to consider the effects of radiative corrections due to the emission of a gluon from the top quark, or a photon from the initial electron/positron. Another recent suggestion has been to try and apply some of these ideas to hadron collisions. Even though we cannot exploit the full power of the reconstruction at hadron colliders (the $t\bar{t}$ are not back-to-back), we can still employ it at the parton level, ignoring the initial non-perturbative QCD effects and fragmentation from the spectator quarks in the p (\bar{p}). In this approximation, we may assume the $t\bar{t}$ are back-to-back, and then we may apply the reconstruction of this analysis.

All of these refinements can be incorporated into the work done in this thesis relatively easily, and the end result will prove very useful to the future experiments at the Next Linear Collider.

References

- [1] For discovery papers, see F. Abe, et al. (CDF Collaboration), *Phys. Rev. Lett.* **74**, 2626 (1995); S. Abachi, et al. (DØ Collaboration), *Phys. Rev. Lett.* **74**, 2632 (1995).
- [2] F. Mandl and G. Shaw, *Quantum Field Theory*, Revised Edition, John Wiley & Sons, 1996.
- [3] S. Parke and Y. Shadmi, *Phys. Lett.* **B387**, 199 (1996); T. Nazuno, *Spin Correlations in Top Quark Production at e^+e^- Linear Colliders* (Doctoral Thesis), Dept. of Physics, Hiroshima U., Japan.
- [4] G. Malhon and S. Parke, *Phys. Rev.* **D53**, 4886 (1996).
- [5] R. Kleiss and W.J. Stirling, *Nuc. Phys.* **B262**, 235 (1985).
- [6] J.J. Sakurai, *Modern Quantum Mechanics*, Revised Edition, Addison-Wesley Publishing Co., 1994.
- [7] M. Jezabek and J.H. Kühn, *Phys. Lett.* **B329**, 317 (1994).
- [8] Thomas Ferbel, personal correspondence.